Supplementary Information: Experimental demonstration of surface and bulk plasmon polaritons in hypergratings

Kandammathe Valiyaveedu Sreekanth[1], Antonio De Luca [2] and Giuseppe Strangi[1, 2 *]

[1]Department of Physics, Case Western Reserve University, 10600 Euclid Avenue, Cleveland (USA)

[2]CNR-IPCF UOS di Cosenza, Licryl Laboratory, Department of Physics, 87036 - Rende (Italy)

*Correspondence author E-mail: gxs284@case.edu (Giuseppe Strangi)

Fabricated Samples

Multilayer samples

The schematic images of the fabricated three different multilayer samples are shown in Fig.S1. Sample 1 (reference): DCM dye mixed PMMA layer (100 nm) on a TiO_2 (10 nm)/glass substrate, sample 2 (control): DCM dye mixed PMMA layer (100 nm) on a TiO_2 (10 nm)/Au (16 nm)/TiO_2 (32 nm)/glass substrate, sample 3 (HMM): DCM dye mixed PMMA layer (100 nm) on a TiO_2 (10 nm)/HMM/glass substrate.

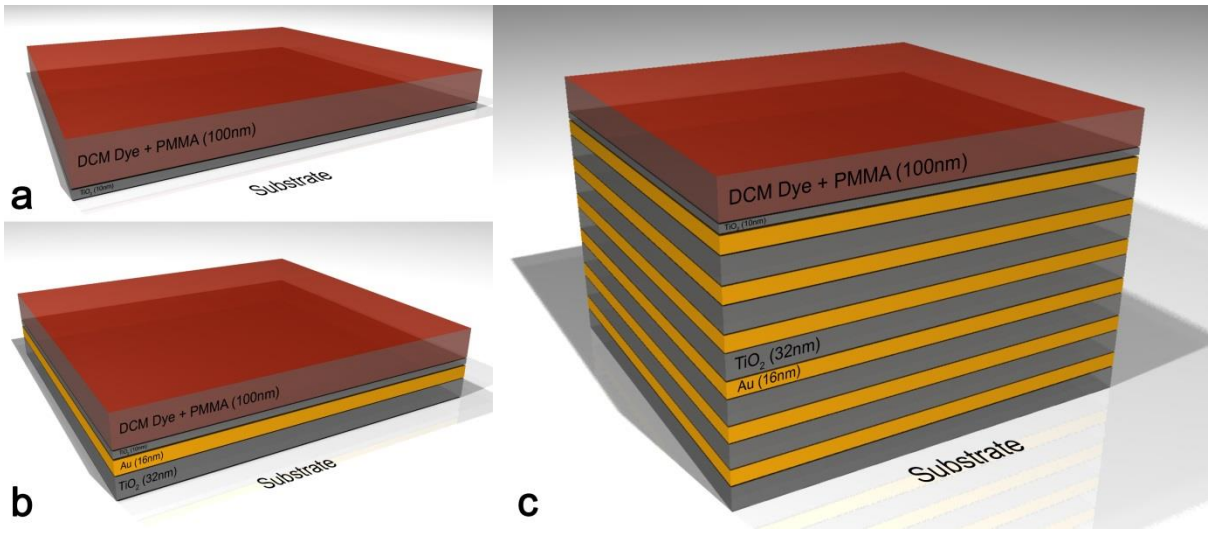

Figure S1 Schematic of (a) reference, (b) control and (c) HMM

Diffraction grating samples

The schematic diagrams of the fabricated six different diffraction grating samples are shown in Fig.S2. Sample 1: Ag layer of thickness 20 nm on a TiO_2 (10 nm)/glass substrate, sample 2 (reference): Metallic (Ag) diffraction grating on a TiO_2 (10 nm)/glass substrate, sample 3 (control): Metallic (Ag) diffraction grating on a TiO_2 (10 nm)/Au (16 nm)/TiO_2 (32 nm)/glass

substrate, sample 4: Metallic (Ag) diffraction grating on a TiO_2 (10 nm)/4x(Au (16 nm)/TiO_2 (32 nm))/glass substrate, sample 5 (hypergrating): Metallic (Ag) diffraction grating on a TiO_2 (10 nm)/HMM/glass substrate and sample 5: Dielectric (PMMA) diffraction grating on a TiO_2 (10 nm)/HMM/glass substrate.

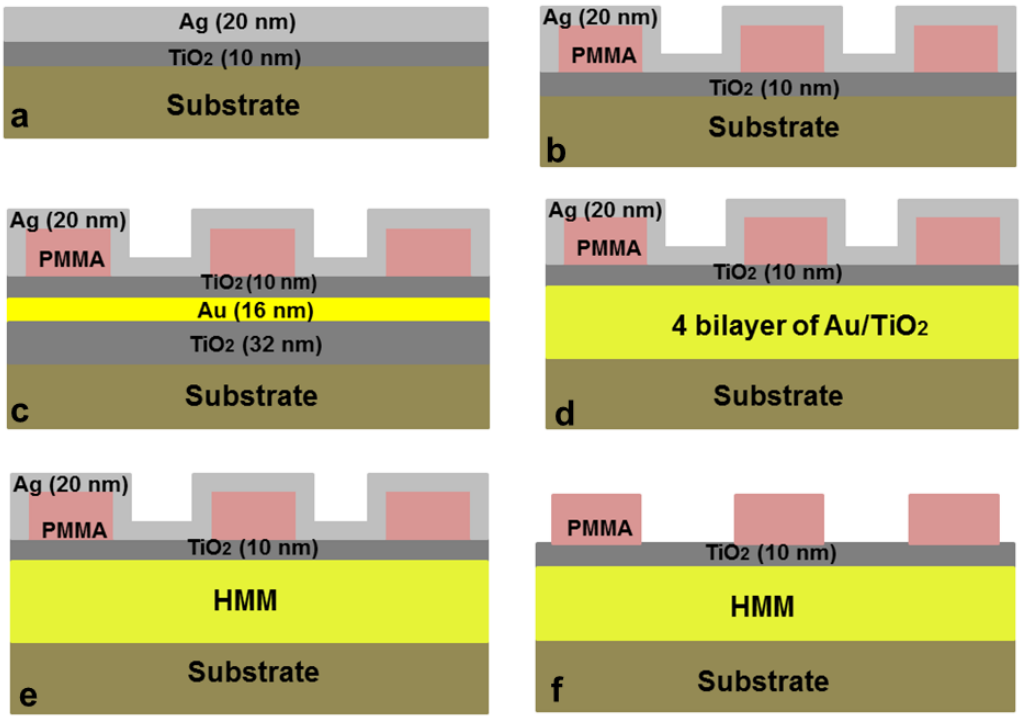

Figure S2 Schematic of (a) sample 1, (b) sample 2 (reference), (c) sample 3 (control), (d) sample 4, (e) sample 5 (hypergrating) and (f) sample 6.

Experiments

Steady state and time-resolved photoluminescence measurements

Figure S3 shows the fluorescent emission spectrum of DCM dye mixed PMMA layer on a glass substrate. The maximum emission wavelength is observed at 620 nm for an excitation wavelength of 450 nm.

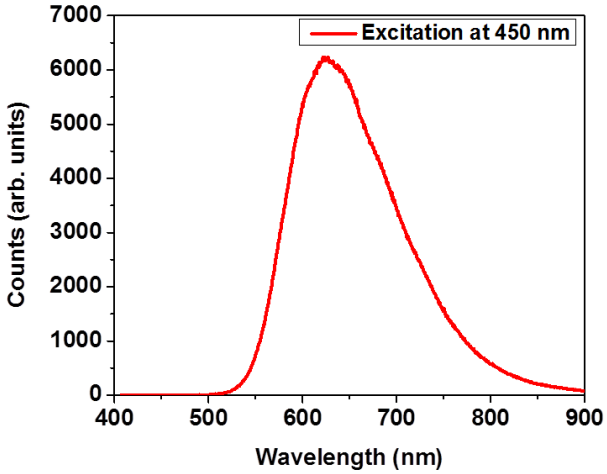

Figure S3 Emission spectrum of DCM dye mixed PMMA layer on a glass substrate

Time-resolved photoluminescence measurements are carried out to obtain the lifetimes of dye on multilayer samples. Figure S4 shows the obtained time decay curves for HMM, control and reference. In order to obtain the lifetime, the data are fitted using, $R(t) = B_1 e^{-t/\tau_1} + B_2 e^{-t/\tau_2} + B_3 e^{-t/\tau_3}$, where τ is the life time. The shortest lifetime (τ_1) is used to plot the results in Fig. 1(c) (main text) because shortest lifetime is related to strong coupling.

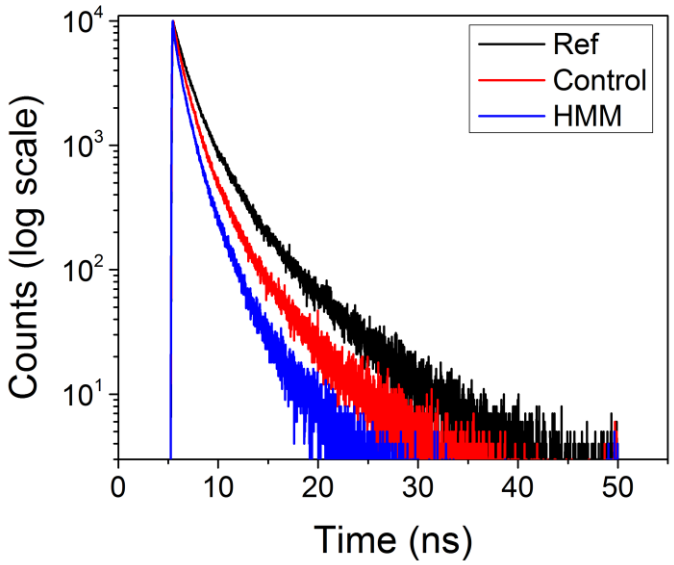

Figure S4 Time-resolved photoluminescence measurements of dye on multilayer samples (HMM, control and reference).

The coupling of dye emission into the metamaterial states is confirmed using steady-state photoluminescence measurements. According to Fig. S5, there is a reduction in photoluminescence intensity from the HMM and this large reduction is due to the preferential emission into high-k metamaterial modes[12].

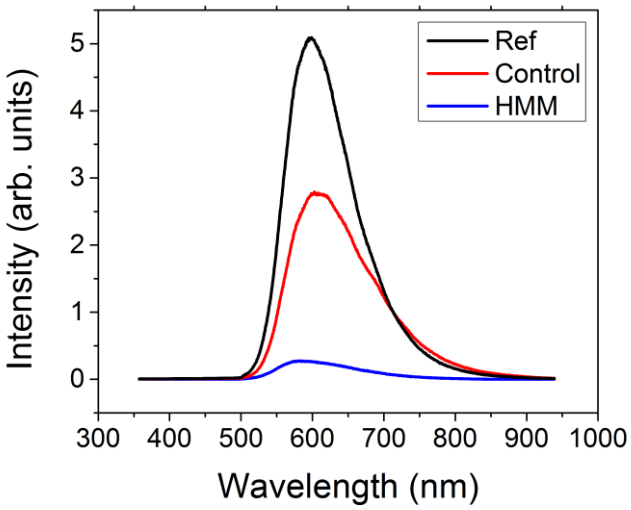

Figure S5 Steady-state Photoluminescence measurements of dye on multilayer samples (HMM, control and reference).

Reflection and transmission measurements

The transmission measurement of diffraction grating samples at normal incidence are carried out and shown in Fig. S6. It is evident from Fig. (a) & (b) that the existence of SPP modes in reference sample and both LRP and GP modes in control sample. However, bulk plasmon modes are not visible in the transmission spectra (Fig. (c) & (d)) at higher wavelengths when the number of bilayer is increased from 4 to 6 (hypergrating). This is due to the large optical loss of Au at higher wavelengths. In order to further support our results, we performed transmission (at normal incidence) and reflection (at oblique incidence) measurements of multilayer (without spacer and PMMA layer) samples (Fig.S7). We could not observe any reflection minima and transmission maxima for the multilayer samples, which strongly

support our findings that the existence of both surface and bulk plasmon modes in hypergrating.

The reflection spectra of hypergrating for different incident angles are shown in Fig. S8. A blue shift in reflectance minima are observed for both surface and bulk plasmon modes when the incident angle is increased. Figure S9 shows the reflectance spectra of hypergrating for three bulk plasmon bands. The decrease in resonance angle is observed when the excitation wavelength is increased in three bulk plasmon bands that show the increase in modal indices of bulk modes with increase of excitation wavelength.

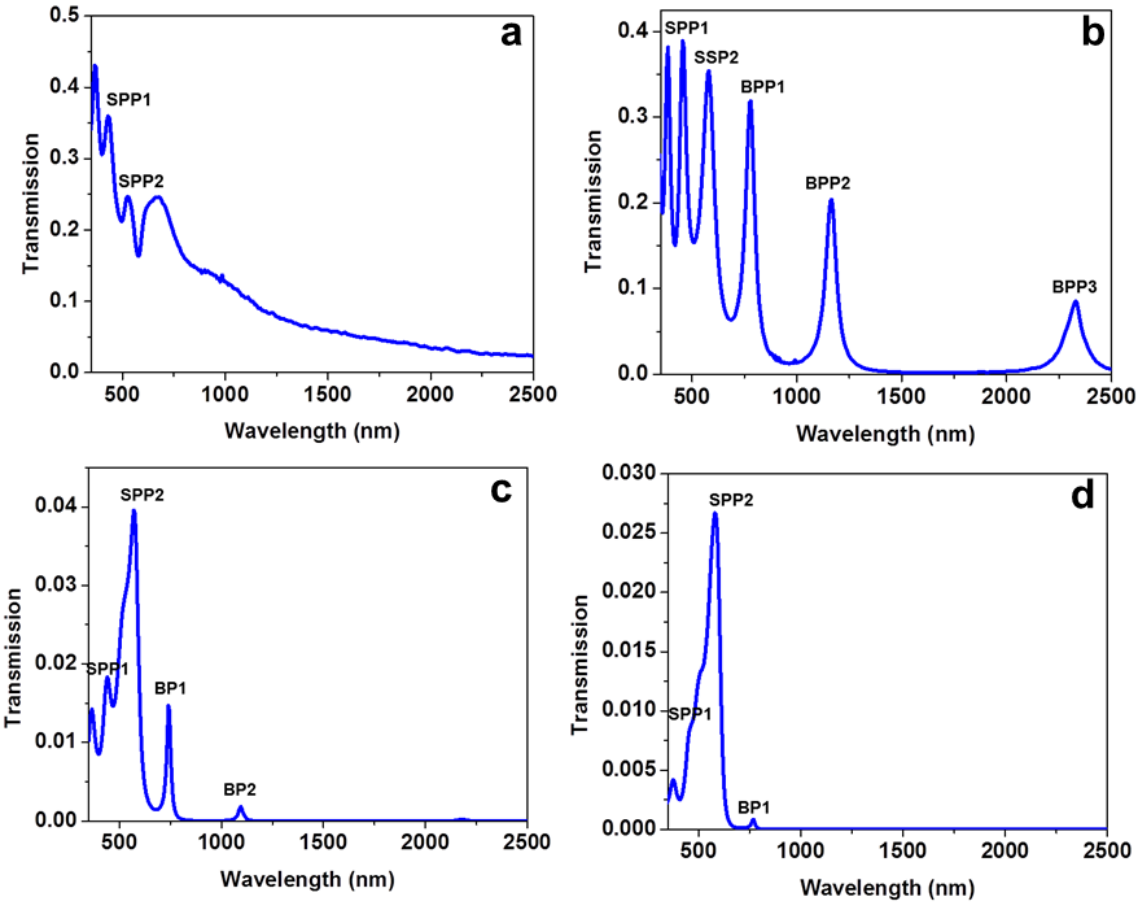

Figure S6 Transmission measurements of diffraction gratings (a) reference, (b) control, (c) 4 bilayer and (d) hypergrating.

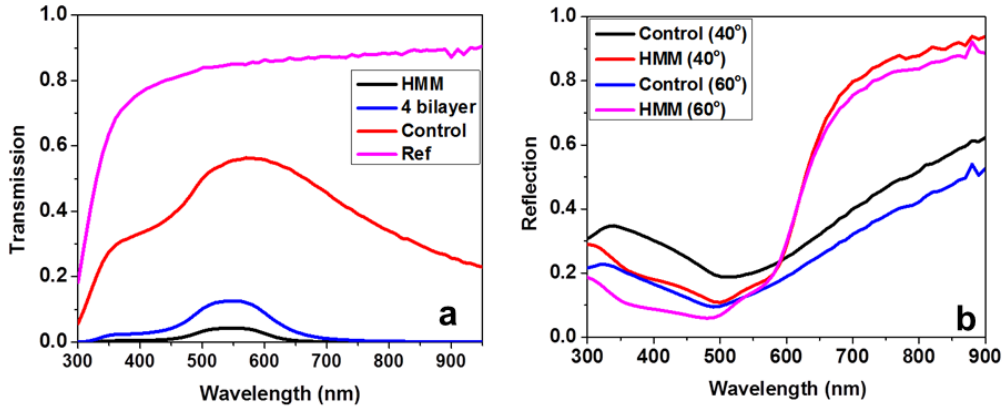

Figure S7 (a) Transmission and (b) reflection measurements of multilayer samples (HMM, control and reference).

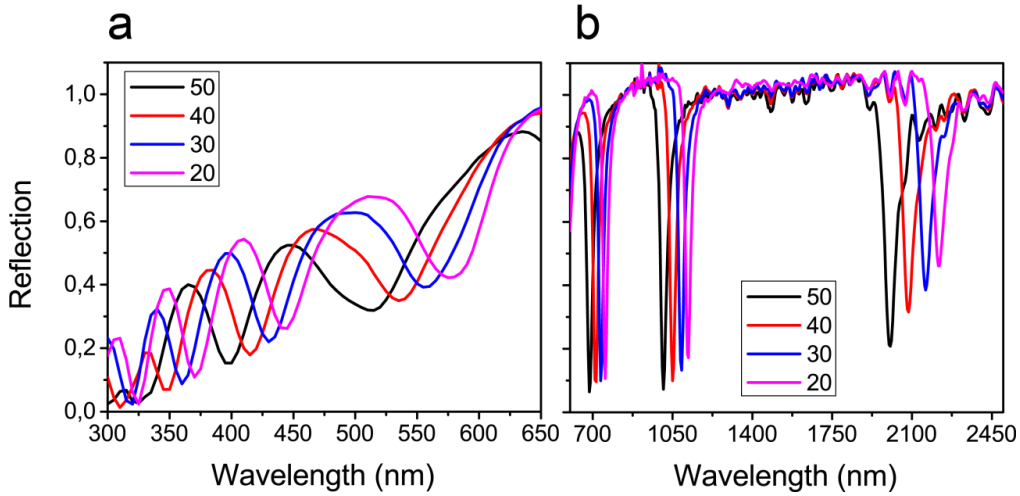

Figure S8 Reflection spectra of hypergrating for different incident angle: (a) for SPP (300-650 nm) & (b) for BPP (700-2450 nm).

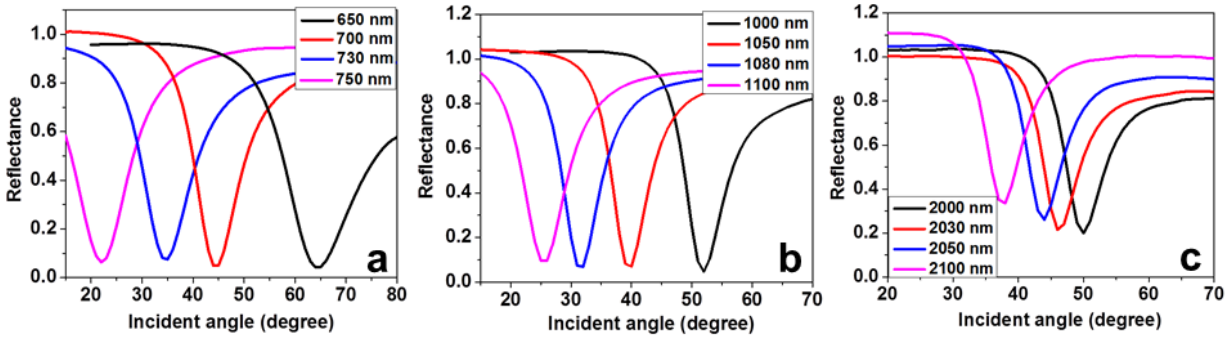

Figure S9 Reflectance spectra (bulk mode distribution) of hypergrating in three plasmon bands such as (a) 650 nm to 750 nm, (b) 1000 nm to1100 nm, and (c) 2000 nm to 2100 nm.

Theoretical analysis of SPP and BPP modes

Dispersion relation

Dispersion relation of SPP and BPP modes given below[29],

For SPP, $k_{SPP} = k_0\sqrt{\varepsilon_d\varepsilon_m/(\varepsilon_d+\varepsilon_m)}$

For BPP, $k_{BPP_N} = k_0\sqrt{\varepsilon_d - \frac{\lambda^2}{\pi^2 t_d t_m}\frac{\varepsilon_d}{\varepsilon_m}}$ for N^{th} order mode

$$k_{BPP_0} = k_0\sqrt{\frac{\varepsilon_d\varepsilon_m(t_d+t_m)}{t_d\varepsilon_m + t_m\varepsilon_d}}$$ for fundamental mode

In the above equations, (t_d, ε_d) and (t_m, ε_m) are the thickness and dielectric permittivity of TiO_2 and Au, respectively. The dispersion plot of SPP and BPP modes are shown in Fig. S10. In Fig. S10, both X and Y axes are normalized with respect to period of the HMM (D=48 nm). Note that N^{th} order mode equation (k_{BPP_N}) is used to plot the BPP mode dispersion in Fig. S10. It is evident from the figure that dispersions of both modes are well beyond the air light line. For shorter wavelength region (above D/λ=0.109 or λ=440 nm), wavevector of SPP modes are higher than that of BPP modes. However, wavevector of BPP modes are higher than that of SPP modes for higher wavelengths. The same behaviour is experimentally observed in Fig. 4 of the manuscript and it is confirmed that the observed reflectance dips at shorter wavelengths (350 nm to 450 nm) are due to SPP modes and at higher wavelengths (650 nm to 750 nm, 1000 nm to 1100 nm and 2000 nm to 2100 nm) are due to BPP modes.

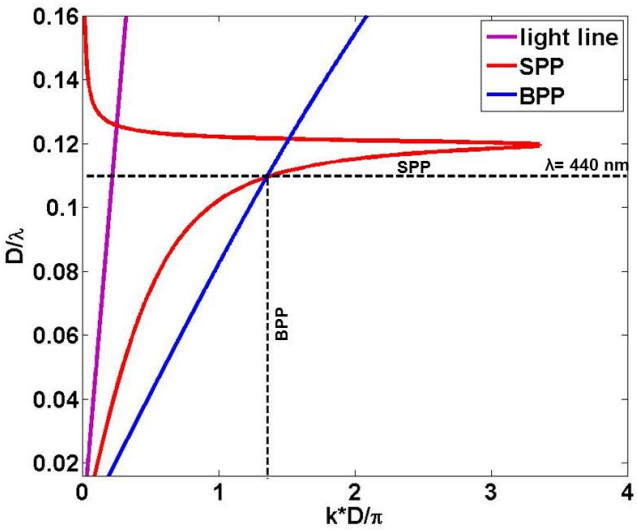

Figure S10 Dispersion relations of SPP and BPP modes. Both X and Y axes are normalized with respect to period (D) of the HMM.

Experimental validation of modal indices of SPP and BPP modes

Since no exact formal theory is available for grating coupling for BPP excitation, we have performed a study on modal index variation with wavelength to experimentally confirm the existence of SPP and BPP modes in our hypergrating structure. Here, experimentally obtained modal indices of both SPP and BPP are compared with the theoretically calculated modal index values.

According to the grating coupling condition, $k_{SPP} = n_0 k_0 \sin\theta + mk_g$ (Here we assumed that the mode is excited based on the +1st diffraction order).

Then the modal index of the mode is given by, $n_{eff} = ((\lambda / \Lambda) + n_0 \sin\theta)$.

Modal indices of SPP modes

The experimentally calculated modal indices of SPP modes are shown in Table 1. It shows that the modal index increases when the wavelength is increased from 350 nm to 400 nm.

Wavelength (nm)	Coupling angle (degree)	Modal index
350	38	1.315
400	60	1.66

Table 1: Modal indices of SPP modes

The modal index of SPP mode is given by,

$$n_{SPP} = \sqrt{\varepsilon_d \varepsilon_m / (\varepsilon_d + \varepsilon_m)}$$

The calculated modal index of SPP using the above equation is shown in Fig. S11a. It is evident from the figure that the SPP modal index increases with wavelength. It shows that the experimental results are well correlated with theory.

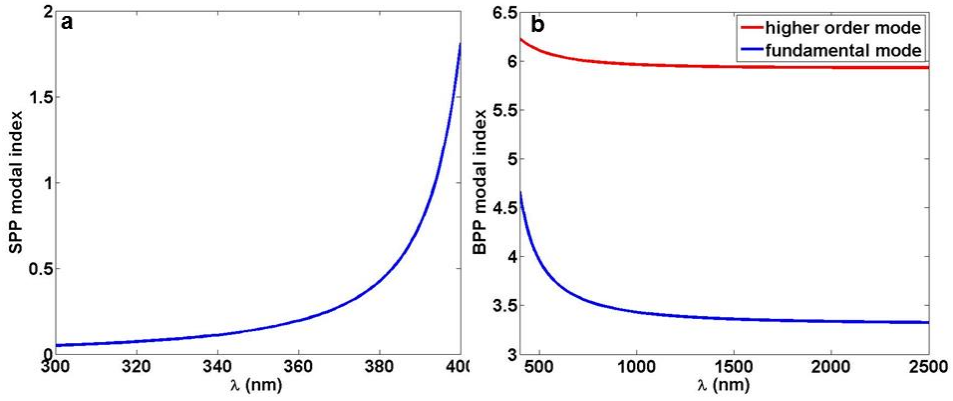

Figure S11 (a) SPP and (b) BPP modal index variation with wavelength.

Modal indices of BPP modes

The experimentally calculated modal indices of BPP modes for three plasmon bands (650 nm to 750 nm, 1000 nm to1100 nm and 2000 nm to 2100 nm) are shown in Table 2. At shorter wavelength bands (650nm to 750 nm and 1000 nm to 1100 nm), modal index decreases with increasing wavelength. However, modal index slightly increases with increasing wavelength at higher wavelength band (2000 nm to 2100 nm).

Wavelength band: 650 nm to 750 nm (Fundamental mode)		
Wavelength (nm)	Coupling angle (degree)	Modal index
650	64	2.2
700	44	2.09
730	34	2.02
750	22	1.87
Wavelength band: 1000 nm to 1100 nm (First order mode)		
Wavelength (nm)	Coupling angle (degree)	Modal index
1000	52	2.8
1050	40	2.74
1080	32	2.7
1100	25	2.62
Wavelength band: 2000 nm to 2100 nm (Second order mode)		
Wavelength (nm)	Coupling angle (degree)	Modal index
2000	50	4.77
2030	46	4.78
2050	44	4.79
2100	38	4.81

Table 2: Modal indices of BPP modes

The modal indices of BPP modes are given by[29] ,

$$n_{BPP_N} = \sqrt{\varepsilon_d - \frac{\lambda^2}{\pi^2 t_d t_m}\frac{\varepsilon_d}{\varepsilon_m}}$$ for Nth order mode

$$n_{BPP_0} = \sqrt{\frac{\varepsilon_d \varepsilon_m (t_d + t_m)}{t_d \varepsilon_m + t_m \varepsilon_d}}$$ for fundamental mode

We then calculated the modal indices of Nth (higher) order and fundamental BPP modes as a function of wavelengths. As shown in Fig. S11b, the modal index of BPP modes decreases with increasing wavelength at shorter wavelengths. However, the modal index of BPP modes slightly vary or constant at higher wavelengths. We have experimentally observed almost same behaviour that modal index decreases with increase of wavelength in two bands (650 nm to 750 nm and 1000 nm to 1100 nm) and modal index slightly varied or almost constant at higher wavelength band (2000 nm to 2100 nm). In particular, we obtained very large resonance angle shift for shorter wavelength band (650 nm to 750 nm) as compared to higher wavelength band (2000 nm to 2100 nm). This large shift is due to the large modal index variation of BPP modes at shorter wavelength region. In the case of BPP modes, the experimental results are in very good agreement with theoretical results.

From the above modal index analysis, we understood that the modal index of BPP modes increases when the wavelength range of the band is increased. Therefore, we consider first band (650 nm to 700 nm) as fundamental modes and other two bands as higher order modes. i. e 1000 nm to1100 nm band is 1st order modes and 2000 nm to 2100 nm band is 2nd order modes.

Numerical simulations

Effective medium theory (EMT)

Since the designed HMM belongs to effective medium approximations, we used effective medium theory to simulate the dielectric permittivity. HMM is an anisotropic medium with uniaxial dielectric tensor components, $\varepsilon_{xx} = \varepsilon_{yy} = \varepsilon_{ll}$ and $\varepsilon_{zz} = \varepsilon_{\perp}$, which are approximated as:

$$\varepsilon_{ll} = \frac{t_m \varepsilon_m + t_d \varepsilon_d}{t_m + t_d}$$

$$\varepsilon_{\perp} = \frac{\varepsilon_m \varepsilon_d (t_m + t_d)}{t_m \varepsilon_d + t_d \varepsilon_m}$$

Here, (t_d, ε_d) and (t_m, ε_m) are the thickness and dielectric permittivity of TiO_2 and Au, respectively. In the simulation, the dielectric constant of TiO_2 is assumed to be 7.3 and the optical constants of Au are calculated based on Drude free-electron theory, $\varepsilon_m = 1 - \left(\frac{\omega_p^2}{\omega(\omega + i/\tau)} \right)$ where ω_p is the plasma frequency of Au and τ is the relaxation time. The thickness of both layers is taken from the experimentally obtained values (16 nm for Au and 32 nm for TiO_2).